

A STUDY INTO GEOPOLYMER CONCRETE USING DIFFERENT TECHNIQUES

Dr.S. CHARLES RUSKIN¹, TEENA JOY², BESSY JOHN³, SHALU ASSIS⁴

Professor¹, Assistant Professor^{2,3,4}

Department of Civil Engineering,

Indira Gandhi Institute of Engineering And Technology

Nellikuzhi P.O, Kothamangalam, Ernakulam (Dist) Pincode 686691

Abstract

Research on the alkali activation of waste materials, such as fly ash, has gained significance because to the potential to produce cost-effective and environmentally friendly cement-like building materials. This study describes the process of activating fly ash using a very alkaline solution. The solutions produced with NaOH and Na₂SiO₃ have the common trait of having a very high concentration of OH⁻ ions. Due to their exceptional strength and mostly non-crystalline microstructure, materials containing latent hydraulic active chemicals activated by alkalis, such as fly ash, are classified as "chemically bonded products." The newly developed environmentally friendly concrete generated during the polymerization of fly ashes demonstrates its amorphous nature with a little amount of crystalline phases.

Keywords: Alkaline liquid, Fly ash, Geopolymer concrete, Scanning electron microscopy (SEM), X-ray diffraction (XRD)

1. Introduction

Geopolymer concrete, which incorporates waste material rich in silica (Si) and alumina (Al) like fly ash, is a favourable substitute due to its significantly reduced greenhouse gas emissions compared to ordinary Portland cement (OPC) concrete. The alkaline activators in geopolymer concrete initiate the formation of a gel by stimulating the silica and alumina found in the source materials. The geopolymer gel acts as a binding agent, bringing together the loose aggregates and any remaining un-reacted components in the mixture, resulting in the formation of geopolymer concrete. The chemical process involved in the synthesis of geopolymer binders differs significantly from that of OPC concrete. The use of modern experimental methods, such as SEM analysis and X-ray Diffraction method, is used to elucidate crucial features of the structure and morphology of these novel materials. A Scanning Electron Microscope (SEM) is an electron microscope that generates pictures of a material by scanning it with a concentrated stream of electrons. The electrons engage in interactions with electrons present in the sample, resulting in

the generation of diverse signals that may be detected and may provide valuable insights about the surface topography and composition of the sample. The electron beam is typically moved in a raster scan pattern, and the location of the beam is coupled with the received signal to generate a picture. Scanning electron microscopy (SEM) is capable of achieving resolutions superior to 1 nm. Specimens may be examined in both high vacuum and low vacuum conditions. Additionally, environmental SEM specimens can be observed in a wet state. X-ray scattering techniques include a group of non-invasive analytical methods that provide insights into the crystal structure, chemical content, and physical characteristics of materials and thin films. These approaches rely on the observation of the dispersed intensity of an X-ray beam as it interacts with a material, taking into account the incident and scattered angle, polarisation, and wavelength or energy. An X-Ray Diffraction (XRD) study was performed to determine the silica phase present in the geopolymer concrete sample. Initially, the specimens were subjected to scanning using an X-ray diffractometer equipped with $\text{CuK}\alpha$ radiation at 40kV / 20 mA. The scanning parameters included a CPS of 1 k, a width of 2.5, a speed of $2^\circ / \text{min}$, and a scanning angle of 2 Theta ranging from 10° to 80° . X-ray diffraction involves the scattering of X-rays by atoms, resulting in a pattern that reveals the lattice spacing of elements in the specimen being analysed. When the X-rays are in phase, they will exhibit constructive interference, resulting in the formation of a peak in the X-ray diffraction pattern at a certain wavelength. The X-ray wavelength is measured over a broad variety of angles to determine the spacing of the material.

2. Experimental

The microstructural studies were conducted using fly ash and geopolymer concrete.

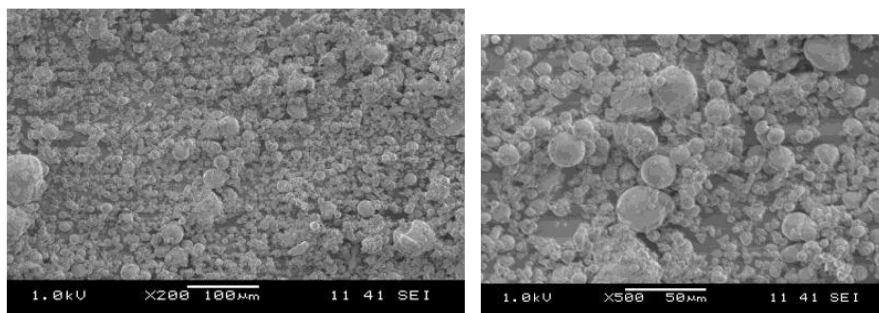
A Scanning Electron Microscope (SEM) uses Back-Scattered Electrons (BSE), which are electrons in the beam that are reflected off the sample due to elastic scattering. Backscattered electrons (BSEs) are often used in analytical scanning electron microscopy (SEM) in conjunction with spectra generated from characteristic X-rays. This is due to the fact that the strength of the BSE signal is closely correlated with the atomic number (Z) of the specimen. Images obtained using backscattered electron (BSE) imaging may provide valuable insights on the spatial distribution of various elements inside the sample. For further analysis, the fly ash sample, OPC, and GPC samples, which had previously undergone compressive strength testing at 28 days, were fragmented into tiny specimens and ground into a fine powder. The resulting powder was then securely stored in air-tight zip lock bags. Subsequently, the specimens were meticulously processed and subjected to analysis using a Scanning Electron Microscope (SEM) to evaluate the microstructure in a qualitative manner. The scanning electron microscope is an invaluable instrument for observing the microstructural evolution of the fly ash and geopolymer concrete matrix specimen.

X-ray diffraction is a method used to qualitatively determine the elements and compounds contained in a sample. An X-ray diffractometer was used to analyse the specimen samples of low calcium fly ash and geopolymer concrete. A minute quantity of test material, in the form of powder, was placed into an aluminium sample container and the surface was then levelled. Subsequently, the sample holder was inserted into the X-ray diffractometer and subjected to analysis throughout the range of 10° to 80° of 2θ angles. The analysis was conducted with a precision of 0.04 degrees and timed for a duration of 3 seconds. The X-ray diffraction examination revealed the presence of several minerals in the samples. The peak intensities of each sample were analysed based on the individual angles discovered in the database.

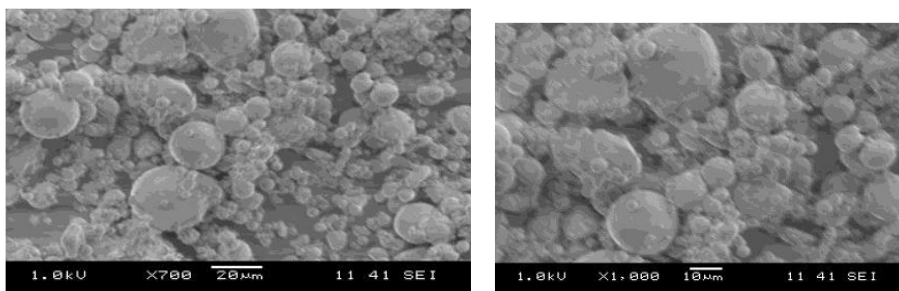
3. Results and Discussions

Figures 1 show the scanning electron microscope (SEM) pictures of fly ash powder at various magnifications. Figure 1(a) shows a micrograph displaying an enlarged picture of fly ash at a magnification of 200. The display exhibits a sequence of spherical and glassy particles with sizes varying from $9\ \mu\text{m}$ to $82\ \mu\text{m}$. The scale bar measures 100 micrometres. Figure 1(b) shows a micrograph displaying a much enlarged picture of fly ash at a magnification of 500. The display indicates the size of the fly ash particles, which vary between $4\ \mu\text{m}$ and $35\ \mu\text{m}$. The particles have a spherical form and the scale bar measures 50 μm . Figure 1(c) is a micrograph displaying a highly enlarged picture of fly ash at a magnification of 700x. The statement denotes the presence of fly ash particles that have a spherical form and fall within the size range of $2.5\ \mu\text{m}$ to $32.5\ \mu\text{m}$. The scale bar measures a length of 20 micrometres. Furthermore, Figure 1(d) depicts a micrograph displaying a magnified picture of the fly ash at a greater magnification of 1000x. The image displays the dimensions of fly ash particles, namely their diameter, which ranges from $7.5\ \mu\text{m}$ to $35\ \mu\text{m}$. The scale bar in the image represents a length of 10 μm .

The SEM pictures in micrographs 1(a) to 1(d) clearly depict the distinctive shape of the original fly ash. The fly ash is composed of various sizes of spherical and vitreous particles, ranging from $7.5\ \mu\text{m}$ to $35\ \mu\text{m}$. The fly ash particles are often empty within, and some spheres may include smaller particles inside them. The spherical shape of fly ash enables the creation of a simple conceptual mixture that can effectively describe the whole process of alkali activation of the ash. It has been noted that almost all fly ash becomes activated, leading to the formation of a compact paste.

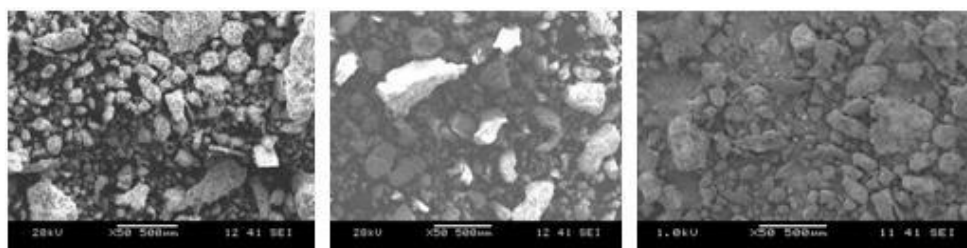


(a) Fly Ash with 200 Magnification (b) Fly Ash with 500 Magnification



(c) Fly Ash with 700 Magnification (d) Fly Ash with 1000 Magnification

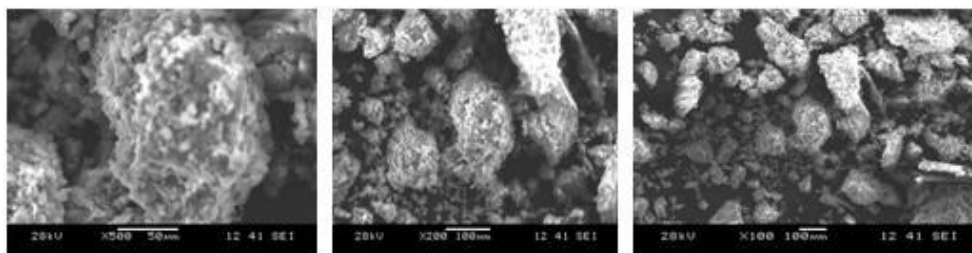
Figure 1 SEM Images of Fly Ash



(a) OPC 20

(b) OPC 30

(c) OPC 40



(d) GPC 20

(e) GPC 30

(f) GPC 40

Figure 2 SEM Images of OPC and GPC for Various Grades

Figure 2 depicts the microstructure picture of regular portland cement concrete and geopolymers concrete samples of different grades, including M20, M30, and M40. Additionally, it showcases the specific measurements of the scale bar and the level of magnification for each grade of OPC and GPC. Figure 2 (a) displays the scanning electron microscope (SEM) picture of OPC (Ordinary Portland Cement) grade 20 at a magnification of 50. The image depicts irregularly shaped particles with lateral dimensions ranging from 100 μm to 400 μm and lengths varying from 400 μm to 1200 μm . The scale bar measures 500 micrometres. These particles have a higher number of empty spaces between each individual particle. Figure 2 (b) shows a micrograph showing an enlarged picture of OPC grade 30 at a 50x magnification. The picture depicts rectangular particles, some of which have unusual shapes. The particles exhibited a range of sizes, with widths ranging from 20 μm to 145 μm and lengths ranging from 62 μm to 790 μm . The scale bar measures 500 micrometres. Furthermore, the micrograph of OPC 30 reveals that the concrete paste has a rather low density. Indeed, it exhibits a little degree of porosity.

Figure 2(c) is a micrograph showing the enlarged picture of OPC of grade 40 at a magnification of 50. The picture displays the particle with an uneven form. The particles exhibited a range of sizes, with diameters ranging from 15 μm to 150 μm . The scale bar measures 500 micrometres. Furthermore, the micrograph of OPC 40 reveals that the concrete paste has a loose packing structure. Figure 2 (d) displays the scanning electron microscope (SEM) picture of grade 20 GPC at a magnification of 500. The picture illustrates that the particles are tightly linked and form a dense layer as a result of the effective polymerization of alkaline solutions with fly ash. The particles exhibited a diameter range of 15 μm to 160 μm . The scale bar measures 50 micrometres. Furthermore, the micrograph of GPC 20 reveals a high degree of compaction in the concrete paste.

Figure 2 (e) shows the scanning electron microscope (SEM) picture of grade 30 GPC at a magnification of 200. The picture illustrates that the particles exhibit a higher viscosity and coalesce into a cohesive mass like a cluster of dense, intertwined threads. The particles exhibited a range of diameters, spanning from 20 μm to 170 μm . The scale bar measures 100 micrometres. Furthermore, the micrograph of GPC 30 reveals a higher level of compaction in the concrete paste compared to the GPC 20 mixture. Micrograph (f) in Figure 2 shows a magnified picture of GPC grade 40 at a 100x magnification. The picture depicts particles that are densely packed and exhibit high viscosity. Additionally, the particles are characterised by uneven shapes. The particles exhibited a range of widths, spanning from 15 μm to 140 μm . The scale bar measures 500 micrometres. Furthermore, the micrograph of OPC 40 reveals that the concrete paste exhibits a higher level of proximity and density compared to the GPC 20 and GPC 30 grade mixes.

Figure 2 demonstrates that the particles of geopolymer concrete have irregular shapes yet are very dense. This geopolymer concrete exhibits a continuous mass of reaction product that resembles a layer of thick fluid that has abruptly solidified, signalling the completion of the polymerization process. The pace at which the activation process occurs, as well as the chemical composition of the resulting products, is influenced by several parameters such as the distribution of particle sizes, the mineral makeup of the fly ash, and the extent to which the activator penetrates. The specimen is a part of the fly ash paste, which is activated by the use of sodium silicate and sodium hydroxide solution. Subsequently, the material undergoes thermal curing at a temperature of 900 degrees Celsius for a duration of 72 hours. The microstructure of the geopolymer concrete seems to be homogeneous and amorphous.

Figure 3 depicts the X-ray diffraction pattern of a sample of low calcium fly ash. In this approach, the 2θ angle is shown on the x-axis, while the intensity of the mineral is depicted on the y-axis. The graph displays the 2θ angle within the range of 0 to 600. The intensity is quantified in numerical counts. An X-Ray Diffraction (XRD) study was performed to identify the silica phase present in the provided sample. This procedure enabled a precise identification of the elements and compounds that were present in the sample. The X-ray diffraction analysis reveals the presence of many minerals in the sample. The minerals that were observed include silica, calcium, alumina, and oxides. The mineral identified in this fly ash sample was Quartz, exhibiting a low level of intensity. The crystal system exhibited a hexagonal structure, with a primitive lattice. The mineral has a molecular weight of 60.08.

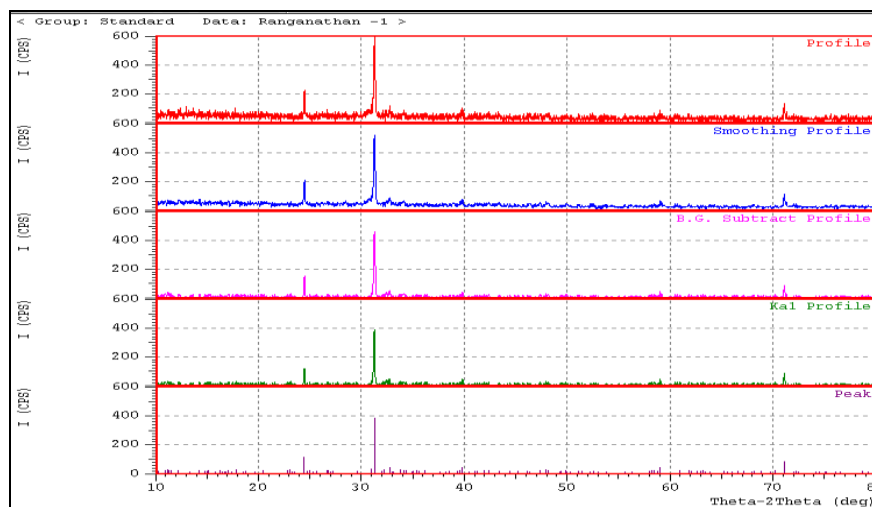


Figure 3: X-Ray Diffraction Pattern of Low Calcium Fly Ash

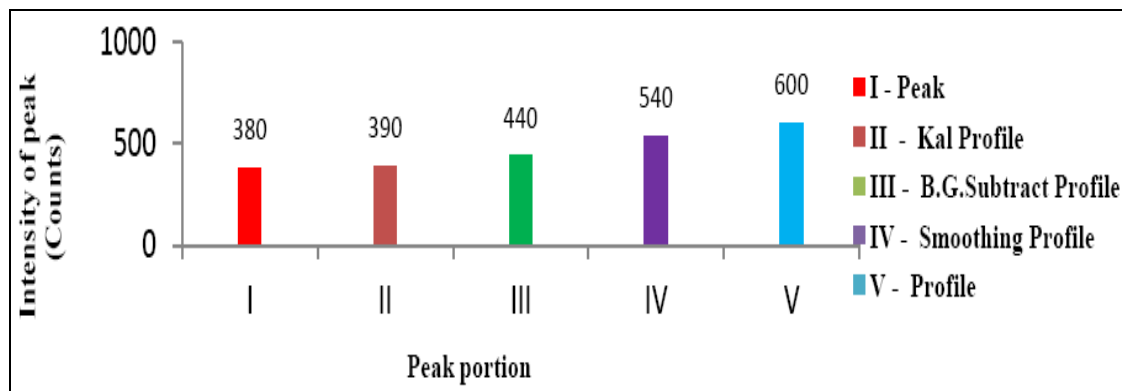


Figure 4: Intensity of Silicon Oxides in Fly Ash Sample

The intensity of silicon oxide in the fly ash sample is displayed in Figure 4 using different sections of the XRD graph. Figure 4 clearly shows that the strength of silicon oxide concentration in fly ash ranges from 380 counts to 600 counts. The V-profile has a silicon oxide intensity that is about 60% higher than the intensity of the I-peak. The V-profile has intensities that are 55% and 37% greater than the II-Kal profile and III-B. G. remove profile intensities. Similarly, the V-profile has an intensity value that is 11% higher than the IV-smoothing profile. Based on these data, it is evident that the intensity of silicon content steadily grew and reached its maximum only at the profile part. Figure 5 displays the X-ray diffraction pattern of the geopolymer concrete powder. This shows that the peak seen indicates the presence of sodium hydroxide and sodium silicate substances in the concrete powder. Based on the X-ray results, the fly ash did not exhibit any crystalline phase when it was treated with solutions of sodium silicate and sodium hydroxide. Therefore, all of the samples, analysed by X-ray diffraction (XRD), had an amorphous component.

Figure 5 depicts the X-ray Diffraction pattern of a sample of geopolymer concrete. The graph displays the 2θ angle, ranging from 10° to 80° , and the intensity, ranging from 0 to 150 counts. Crystalline form of the mineral NaOH was found to be more prevalent in this graph. The crystal system exhibited an orthorhombic structure. The lattice exhibited end-centered structure. The mineral has a molecular weight of 40.00. Its volume, represented by CD, is 131.47, and its Dx value is 2.021. The presence of NaOH in crystalline form was indicated by the peaks seen at 2θ angles of 31° , 34° , and 37° . The presence of sodium hydroxide in its crystalline form was indicated by these peaks, while other smaller peaks indicated the presence of other oxide compounds in the sample.

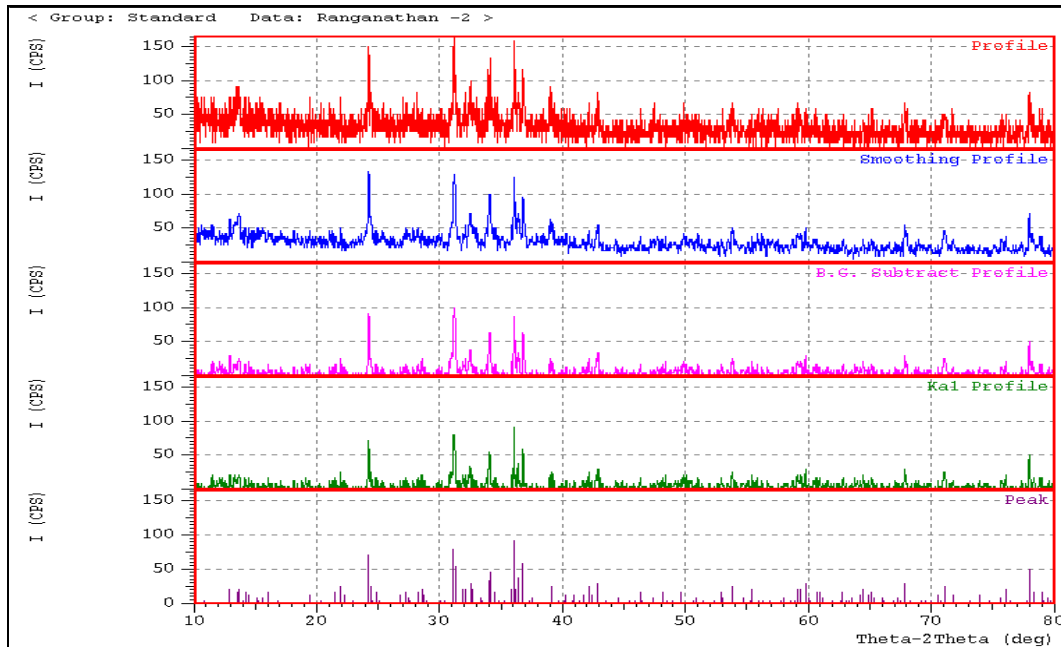


Figure 5: X-Ray Diffraction Pattern of Geopolymer Concrete

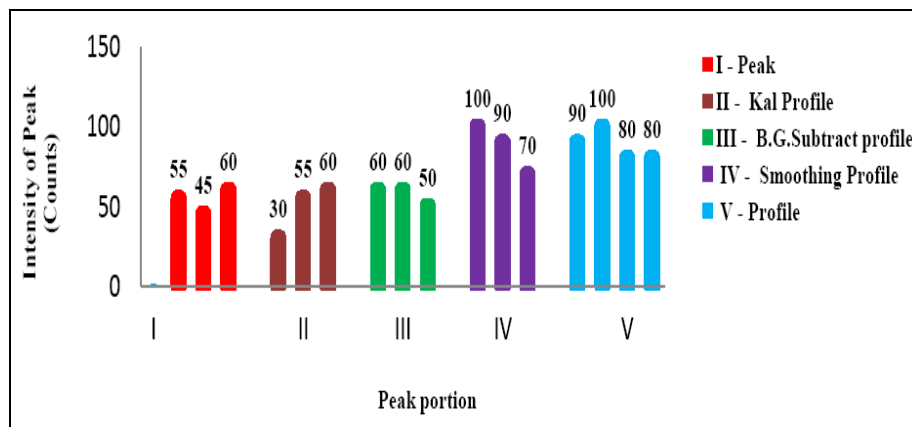


Figure 6: Intensity of Sodium Hydroxide in Geopolymer Concrete Sample

The XRD graph displays the intensity of sodium hydroxide in the geopolymer concrete sample, as seen in Figure 6. Figure 6 demonstrates that the sodium hydroxide content intensity of geopolymer concrete varied between 30 counts and 100 counts. The V-profile demonstrates that the intensity of silicon oxide is about 70% more than the intensity of the I-peak. Additionally, the V-profile exhibits intensities that are 80% and 60% greater than those of the II-Kal profile and III-B. G. subtract profile, respectively. Similarly, the V-profile has a 4% higher value compared

to the IV-smoothing profile intensity. Based on these data, it has been shown that the concentration of sodium hydroxide rose exclusively in the IV-smoothing profile and V-profile regions, reaching its maximum concentration in the profile portion.

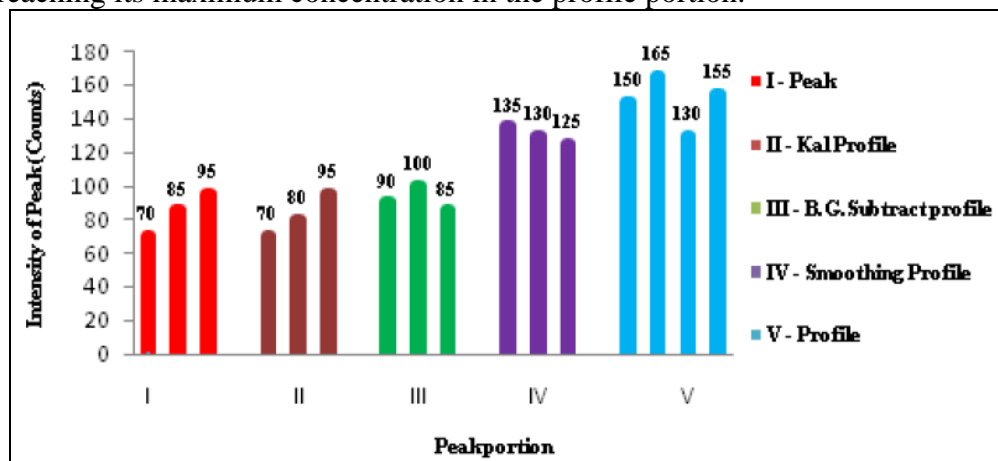


Figure 7: Intensity of Sodium Silicate in Geopolymer Concrete Sample

The XRD graph displays the intensity of sodium silicate in the geopolymer concrete sample, as seen in Figure 7. The sodium silicate component of geopolymer concrete varied between 70 counts and 165 counts, indicating different levels of intensity. The V-profile has a silicon oxide intensity that is about 90% higher than the intensity of the I-peak. Additionally, the V-profile exhibits intensities that are 78% and 72% greater than the II-Kal profile and III-B. G. remove profile intensities. Similarly, the V-profile has an intensity value that is 21% higher than the IV-smoothing profile. Based on these data, it is evident that the intensity of sodium silicate content rose primarily in the IV-smoothing profile and V-profile sections, reaching its maximum just in the profile component.

4. Conclusion

The following findings have been derived from the experimental experiments.

- The SEM figure clearly shows the distinct microstructural variations between fly ash and geopolymer concrete.
- The fly ash particles have a diameter ranging from 10 to 200 micrometres and are spherical in form.
- The scanning electron microscope (SEM) picture of the fly ash reveals a compact structure, suggesting successful alkali activation of the fly ash.

- The scanning electron microscope (SEM) picture of standard Portland cement concrete reveals that the microstructure of the concrete is characterised by porosity and a relatively low density.
- The scanning electron microscope (SEM) picture of geopolymer concrete reveals a well-formed and dense microstructure, providing evidence of the successful polymerization process.
- During XRD examination, the fly ash sample exhibits the presence of silicon oxide at an angle of 2θ , specifically at 32° , with an intensity of 600 counts.
- The geopolymer concrete sample contains sodium hydroxide chemical with a peak intensity of 100 counts at 2θ angles of 34° and 36° .
- In the geopolymer concrete sample, the sodium silicate exhibits a peak intensity of 165 counts at an angle of 32° (2θ).

5. References

- [1]. Djwanto Hardjito and Steenie, E. Wallah, “Development of Fly ash-based Geopolymer Concrete”, ACI Materials Journal, 101(6), 2004, 467-472
- [2]. Davidovits, J. “Global Warming Impact on the Cement and Aggregates Industries”, World Resource Review, 6(2), 1994, 263-278
- [3]. Douglas C. Comrie, John H. Paterson and Douglas J. Ritcey, “Applications of Geopolymer Technology to its stabilization”, D. Comrie consulting Ltd, 120 Traders Boulevard east, Suite 209, Mississauga, Ontario, L4Z 2H7, 1998, 161-165
- [4]. Fernandez Jimenez, A., Palomo, A. and Criado, M., “Microstructure development of alkali-activated fly ash cement: a descriptive model”, Cement and Concrete Research, 34(6), 2004, 1204-1209
- [5]. Fernandez Jimenez, A.M. and De La Torre, A.G., “Quantitative determination of Phases in the alkali activation of fly ash Part I”, Potential Ash Reactivity, Fuel, 85(5-6), 2006, 625-634
- [6]. Frantisek Skvara, Tomas Jilek and Lubomir Kopecky, “Geopolymer materials based on Fly ash”, Ceramics Silika, 49(3), 2005, 195-204
- [7]. Frantisek Skvara, “Alkali activated materials or Geopolymers”, Lecture notes, Department of Glass and Ceramics, Institute of Chemical Technology, Prague, 2007, 173-177
- [8]. Jain, L.K. “Fly ash in cement and concrete: what experts say”, The Indian Concrete Journal, 77(4), 2003, 49-58
- [9]. Jo, B.W., Park, S.K. and Moon, R.G. “Properties of clinker-free mortar based on chemically bonded municipal solid ISTE incinerator ash”, Magazine of Concrete Research, 60(5), 2008, 323-328

- [10]. Mehta, P.K. and Monteiro, P.J.M., “Concrete: Microstructure, Properties and Materials”, Third Edition., McGraw Hill, New York, 2005
- [11]. Amran YM, Alyousef R, Alabduljabbar H, El-Zeadani M. Clean production and properties of geopolymer concrete; A review. Journal of Cleaner Production. 2020 Apr 1;251:119679.
- [12]. Raijiwala, D.B. and Patil, H.S. “Geopolymer concrete: A concrete of next decade”, Journal of Engineering Research and Studies, 2(2), 2011, 19-25
- [13]. Li N, Shi C, Zhang Z, Wang H, Liu Y. A review on mixture design methods for geopolymer concrete. Composites Part B: Engineering. 2019 Dec 1;178:107490.
- [14]. Hassan A, Arif M, Shariq M. A review of properties and behaviour of reinforced geopolymer concrete structural elements-A clean technology option for sustainable development. Journal of Cleaner Production. 2020 Feb 1;245:118762.
- [15]. Cui Y, Gao K, Zhang P. Experimental and statistical study on mechanical characteristics of geopolymer concrete. Materials. 2020 Apr 2;13(7):1651.